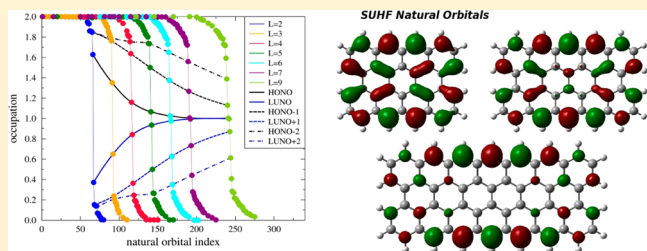


Entanglement and Polyradical Character of Polycyclic Aromatic Hydrocarbons Predicted by Projected Hartree–Fock Theory

Pablo Rivero,^{*,†} Carlos A. Jiménez-Hoyos,[†] and Gustavo E. Scuseria^{†,‡}[†]Department of Chemistry and [‡]Department of Physics and Astronomy, Rice University, Houston, Texas 77005-1892, United States

ABSTRACT: We study strong correlation effects in a series of fused benzene rings (acenes) of varying length and width using our recently developed projected Hartree–Fock (PHF) method. These molecules, commonly known as polycyclic aromatic hydrocarbons or nanographenes, are very challenging for electronic structure theory because of their strong multireference character. This challenge is here met by PHF at moderate computational cost optimizing a spin eigenfunction obtained by projection of an unrestricted Hartree–Fock (UHF) trial determinant. The resulting method, known as SUHF, predicts that polyyradical behavior and orbital entanglement are enhanced with molecular size, especially in systems whose structural motifs are dominated by zigzag edges, like oligoacenes.



INTRODUCTION

Polycyclic aromatic hydrocarbons¹ (PAHs), also known as nanographenes, belong to a class of organic molecules made of fused benzene rings containing only carbon and hydrogen atoms. The electronic structure of PAHs systems is largely determined by the delocalization of π electrons. Oligoacenes (also referred to as polyacenes) are made of linearly fused acenes. They usually have singlet ground-state configurations for all chain lengths.^{2–5} There has been enormous theoretical⁶ and experimental interest in these systems due to their intriguing electronic properties⁷ as well as their carcinogenic, mutagenic, and potent immunosuppressant effects.⁸ Oligoacenes with one, two, and three acenes (from benzene to anthracene) are the smallest and most abundant in nature because of their stability. Pentacene has been one of the most widely studied organic semiconductors for thin field transistors because of its high charge carrier mobility.⁹ Hexacene and heptacene have lower stability and poorer solubility.^{10,11} A few recent theoretical studies have focused on large PAHs,^{3,12,13} particularly on the properties that an increasingly longer conjugation length may confer compared with those of carbon nanotubes or graphene. These larger PAHs also display an extraordinarily high thermal conductivity as well as interesting mechanical and electrical properties.^{14,15}

The electronic ground state and reactivity of PAHs has a strong dependence on the structure of their edges,¹⁶ which can be of a zigzag or armchair nature. In this sense, these molecules share many properties with graphene nanoribbons and other carbon nanostructures.^{17–19} Their length and width (in terms of the number of fused acenes) is also expected to influence their polyyradical character. We here define polyyradical character based on the number of natural occupations (eigenvalues of the correlated one-body density matrix) that are close to one, or more precisely, when they belong—in our definition—to the somewhat arbitrary range of [0.5,1.5]. Polyyradical character in

PAHs is a consequence of multireference character and strong correlation, and thus these concepts are closely connected.

The inability of DFT functionals to correctly describe polyyradical character in PAHs^{20,21} leaves important questions unanswered that can only be addressed by electronic structure methods using multiconfigurational wave functions.^{2,22} There are currently only a handful of multireference ab initio methods for studying the electronic properties of large PAHs where polyyradical character becomes pervasive. Complete and restricted active space calculations are feasible only on relatively small systems²³ compared with the molecular sizes that we are interested here in studying. The variational two-electron reduced density matrix (2-RDM) method^{24–26} has been applied^{12,27} to 2D arrangement of rings. However, this method cannot currently treat large PAHs, as their authors concede.¹² Other newly developed multireference methods, namely, the density-matrix renormalization group (DMRG) algorithm^{3,28} as well as the multireference averaged quadratic coupled cluster method (MR-AQCC),²⁹ have been employed to study large PAHs.

Our recently developed projected Hartree–Fock (PHF) method³⁰ in its spin-projected variant (SUHF) is here used as a novel alternative multireference method capable of capturing strong correlation effects associated with spin fluctuations while retaining the low (mean-field) computational cost typical of Hartree–Fock calculations.³¹ This allows us to study here systems containing more than 25 fused rings, much larger than previous multireference wave function studies. The PHF wave function is obtained by restoring symmetries and good

Special Issue: Peter G. Wolynes Festschrift

Received: February 10, 2013

Revised: April 14, 2013

quantum numbers from a broken symmetry trial wave function. This symmetry breaking and restoration methodology yields a fairly sophisticated multiconfigurational wave function that is a linear combination of nonorthogonal determinants based on a single broken symmetry HF state. The recent application of PHF to copper oxide cores³² and the 2D Hubbard model³³ has confirmed its usefulness in strongly correlated systems. Because it is a variational wave function method, PHF rests on a firm theoretical footing and can thus address systems where DFT fails. At the same time, the fact that the PHF wave function is fully determined by a single Slater determinant (despite its multireference character) leads to a simple and direct interpretation of results in terms of a molecular orbital picture. PHF correlates all electrons and does not require a preselection of an active orbital space either by chemical intuition or by an energy criterion. The basis-set dependence of PHF is similar to that of CAS and much less severe than coupled-cluster theory. All of these attributes make PHF ideal for studying fairly large systems compared with other techniques.

The aim of this article is to investigate the orbital entanglement and polyyradical character of PAHs, particularly in connection with their structural motif and molecular size. To quantify these properties, we compute the spin-projected SUHF natural occupations (eigenvalues of the projected one-body density matrix) and the von Neumann entropy³⁴ as a measure of entanglement. Results obtained in this article show that polyyradical behavior and orbital entanglement are enhanced with increasing number of linearly fused acenes, especially in systems where zigzag edges are predominant like oligoacenes.

THEORY

In this section we describe the most salient features of PHF theory. In fact, the PHF approach was introduced in quantum chemistry more than 40 years ago^{35,36} but after two decades of intensive research, the idea was mostly abandoned.³⁷ We have recently presented a novel, efficient approach to carry out the optimization of PHF wave functions in a variation-after-projection (VAP) manner (ref 30.). A key aspect of our formulation is the use of one-body spin operators to enforce rotational invariance of the wave function in spin space, as opposed to the approach advocated by Löwdin,³⁵ who employed a projection operator written as a product of two-body operators to extract the desired spin component. We note that the projection-after-variation (PAV) approach (where a single-shot projection is done after an unrestricted optimization) is much less reliable than VAP; the former may lead, for instance, to unphysical dissociation curves that complicate the evaluation of properties.³⁸ Previous work³⁹ has shown the importance of restoring spin symmetry from a broken-symmetry HF state, although the calculations were performed with a PAV scheme.

In this article, we use the spin-projected unrestricted Hartree–Fock method (SUHF) which is a particular case of PHF based on an underlying UHF broken symmetry Slater determinant $|\Phi_{\text{UHF}}\rangle$. We construct a state $|\Psi^{sm}\rangle$ with good s and m quantum numbers, that is

$$\hat{S}^2 |\Psi^{sm}\rangle = s(s+1) |\Psi^{sm}\rangle \quad (1)$$

$$\hat{S}_Z |\Psi^{sm}\rangle = m |\Psi^{sm}\rangle \quad (2)$$

by application of a projector operator \hat{P}_{mm}^s to $|\Phi_{\text{UHF}}\rangle$ as follows

$$|\Psi^{sm}\rangle = \hat{P}_{mm}^s |\Phi_{\text{UHF}}\rangle \quad (3)$$

$$\hat{P}_{mm}^s = \frac{2s+1}{8\pi^2} \int d\Omega [D_{mm}^s(\Omega)]^* \hat{R}(\Omega) \quad (4)$$

Here $D_{mm}^s(\Omega) = \langle sm | R(\Omega) | sm \rangle$ is the standard Wigner D-matrix and $\hat{R}(\Omega) = e^{-ia\hat{S}_x} e^{-ib\hat{S}_y} e^{-ic\hat{S}_z}$ is the spin rotation operator defined in terms of the set of Euler angles $\Omega = (\alpha, \beta, \gamma)$.

We variationally optimize the energy of a wave function of the form 3. That is, we minimize the functional

$$E[\Phi_{\text{UHF}}] = \frac{\langle \Psi^{sm} | \hat{H} | \Psi^{sm} \rangle}{\langle \Psi^{sm} | \Psi^{sm} \rangle} = \frac{\langle \Phi^{sm} | \hat{H} \hat{P}_{mm}^s | \Phi^{sm} \rangle}{\langle \Phi^{sm} | \hat{P}_{mm}^s | \Phi^{sm} \rangle} \quad (5)$$

where we have used the fact that the projection operator \hat{P}_{mm}^s is Hermitian and idempotent and commutes with the Hamiltonian. Details of the optimization can be found in ref 30.

We note that because $|\Phi_{\text{UHF}}\rangle$ preserves S_Z symmetry, the integrations over α and γ in eq 5 can be trivially carried out. The energy functional becomes

$$E[\Phi_{\text{UHF}}] = \frac{\int d\beta \sin \beta d_{mm}^s(\beta) \langle \Phi_{\text{UHF}} | \hat{H} e^{-i\beta S_y} | \Phi_{\text{UHF}} \rangle}{\int d\beta \sin \beta d_{mm}^s(\beta) \langle \Phi_{\text{UHF}} | e^{-i\beta S_y} | \Phi_{\text{UHF}} \rangle} \quad (6)$$

where $d_{mm}^s(\beta) = \langle sm | e^{-i\beta S_y} | sm \rangle$ is Wigner's small d matrix.

Before closing this section we would like to briefly discuss the way in which natural occupations are computed. We obtain them by diagonalization of the one-particle reduced-density matrix (1-RDM), γ , of the projected Hartree–Fock state:

$$\gamma_{i,j} = \frac{\langle \phi | \hat{P}_{mm}^s a_j^\dagger a_i \hat{P}_{mm}^s | \phi \rangle}{\langle \phi | \hat{P}_{mm}^s \hat{P}_{mm}^s | \phi \rangle} \quad (7)$$

In ref 40, we mentioned that because operators of the form $a_j^\dagger a_i$ do not in general commute with \hat{P}_{mm}^s one needs to perform double integration over the Euler angles. In fact, one can use the Wigner–Eckart theorem to evaluate density matrices with a single projection operator. In particular, if T_q^k is a rank- k tensor operator, then it is easy to show that:⁴¹

$$\begin{aligned} \hat{P}_{mm}^s T_q^k \hat{P}_{mm}^s &= \delta_{q,0} \langle smk0lsm \rangle \\ &\times \sum_{\mu'} (-1)^{\mu'} \langle s, m, k, -\mu' | s, m - \mu' \rangle T_{\mu'}^k \hat{P}_{m-\mu',m}^s \end{aligned} \quad (8)$$

where $\langle j_1 m_1 j_2 m_2 | j m \rangle$ are Clebsch–Gordan coefficients.

Harriman⁴² has discussed many of the properties of the 1-RDM for wave functions of the form of eq 3, that is, SUHF wave functions. Some notorious features include:

- There are at most $2N$ eigenvalues different from 0, where N is the number of electrons.
- The natural orbitals of the spin and charge density matrices are the same in the projected and unprojected states, that is, $|\Psi^{sm}\rangle$ and $|\Phi_{\text{UHF}}\rangle$.
- The eigenvalues of the 1-RDM appear in “corresponding pairs” in the sense that one can always find indices j and k such that $n_{j\uparrow} + n_{k\downarrow} = 1$. Here $n_{j\uparrow}$ is the j th natural occupation of spin \uparrow .

A major drawback of the PHF approach is its lack of size extensivity. This means that the correlation energy per particle (with respect to UHF) decays to zero as a function of system size. The wave function and other properties remain, nevertheless, different. We here explore whether for large systems the UHF and SUHF natural occupations become

similar. In particular, we compare the eigenvalues of the UHF charge density matrix ($D = \rho_{\uparrow} + \rho_{\downarrow}$) with the correlated natural occupations obtained as eigenvalues of the true SUHF density matrix.

COMPUTATIONAL DETAILS

To investigate the relationship between polyyradical character, structural motif, and molecular size, we have carried out a series of singlet SUHF calculations on PAHs featuring different width (W) and length (L). Representative structures among the largest studied in this work are listed in Table 1. Figure 1 graphically describes our adopted definition for acene width (W) and length (L).

Table 1. Representative Systems among the Largest Studied in This Paper^a

L	W	formula	number of basis functions	basis set
12	1	$C_{50}H_{28}$	1118	6-31++G(d,p)
10	1	$C_{42}H_{24}$	942	
4	4	$C_{72}H_{24}$	696	6-31G
9	2	$C_{76}H_{26}$	736	
2	6	$C_{60}H_{28}$	596	

^a L and W correspond to the acene length and width, respectively.

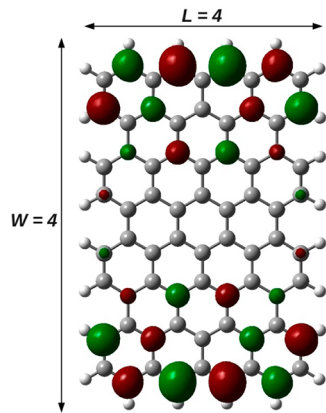


Figure 1. Adopted definition for W (width) and L (length) is here displayed for $C_{72}H_{24}$. The highest occupied natural orbital (HONO) is plotted showing a preference for zigzag over armchair edges. (See the discussion in the text.)

We study chains with 1 to 12 linearly fused benzenes ($L = 1-12$) and width of 1 ($W = 1$) acene resulting in structural motifs dominated by zigzag edges. For systems with two strips ($W = 2$), we have considered chains from 2 to 9 linearly fused benzenes ($L = 2-9$) that also result in structures dominated by zigzag edges. Systems with armchair edges are generated by considering $L = 2$ and chains with one to six acenes of width ($W = 1-6$). The dependence of the orbital entanglement on molecular size and structure is assessed in terms of natural orbital occupations and quantified by means of the symmetrized von Neumann entropy.

All calculations were carried out using a locally modified version of the Gaussian⁴³ suite of programs. Self-consistent field convergence was aided via the DIIS extrapolation technique.^{44,45} Molecular geometries were optimized with B3LYP/6-31++G(d,p); in all cases, the B3LYP solutions are stable with respect to spin symmetry breaking; that is, B3LYP converges to

a solution with $\langle \hat{S}^2 \rangle = 0$. The projected wave functions are chosen as singlet spin eigenfunctions. Initial SUHF calculations were performed using a 6-31++G(d,p) basis for the systems referred to as $W = 1$ and $L = 1-12$. A smaller basis set (6-31G) was used for the rest after determining (see Figure 2) that it

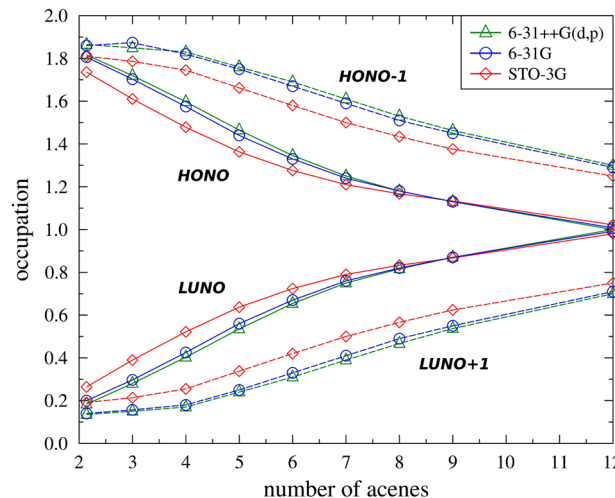


Figure 2. SUHF natural occupations as a function of basis set and number of acenes for zigzag structures with $W = 1$.

leads to SUHF occupations similar to those obtained in the larger basis set. Note, however, that minimal basis (STO-3G) results presented in Figure 2 show appreciable deviations for all systems with respect to larger basis set data and therefore the STO-3G basis set cannot be deemed reliable. In all cases, we have evaluated the integral in eq 6 with enough accuracy to obtain $\langle \hat{S}^2 \rangle$ correct to a precision of 10^{-5} or better. We emphasize that none of our SUHF calculations uses an active space restriction.

RESULTS AND DISCUSSION

DMRG and variational 2-RDM approaches have so far been the only electronic structure methods used to explore the polyyradical character of large PAHs. Mizukami et al.²⁸ (DMRG) and Pelzer et al.¹³ (2-RDM) have confirmed the important role of geometry in determining multireference character. Because of their computational scaling, these two methods have some limitations on system size and basis set. In fact, most previous studies have used minimal basis sets; our own SUHF results indicate that larger basis may be required to describe these systems accurately. We here report results on larger structures with larger basis sets and, when adequate, compare with previous studies.

To quantify orbital entanglement and how it is influenced by structural motif and size, we have computed natural occupations using our SUHF method. These occupations span the interval [0,2], that is, from zero occupation to double-occupancy. To help scrutinize polyyradical character, we have connected natural orbitals with occupations in the range [0.5,1.5] with lines in our plots. We follow previous authors^{24,29} in denoting highest occupied natural orbital (HONO) and lowest unoccupied natural orbital (LUNO), the natural orbitals with index $N_e/2$ and $N_e/2 + 1$, respectively, where N_e is the number of electrons, which corresponds to the HOMO and LUMO of Hartree–Fock theory. However, one should note that any NO with a nonzero occupation is, strictly speaking,

Table 2. Comparison between CASSCF, SUHF, and SGHF³⁰ Energies and Natural Occupations for Benzene, Naphthalene, and Anthracene Using the STO-3G Basis Set^a

	benzene			naphthalene			anthracene		
	E (au)	HONO	LUNO	E (au)	HONO	LUNO	E (au)	HONO	LUNO
CAS	-227.997	1.86	0.14	-378.863	1.82	0.19	-529.722	1.77	0.24
SUHF*	-227.984	1.85	0.15	-378.812	1.77	0.23	-529.630	1.66	0.34
SUHF	-228.020	1.83	0.17	-378.854	1.74	0.26	-529.678	1.61	0.39
SGHF	-228.063	1.84	0.15	-378.909	1.78	0.22	-529.742	1.67	0.33

^aSUHF* is used to denote SUHF calculations with an active space; the number of active electrons and active orbitals is determined by the number of π orbitals. In CASSCF calculations, we have used symmetry to determine the orbitals included in the active space (the full π system).

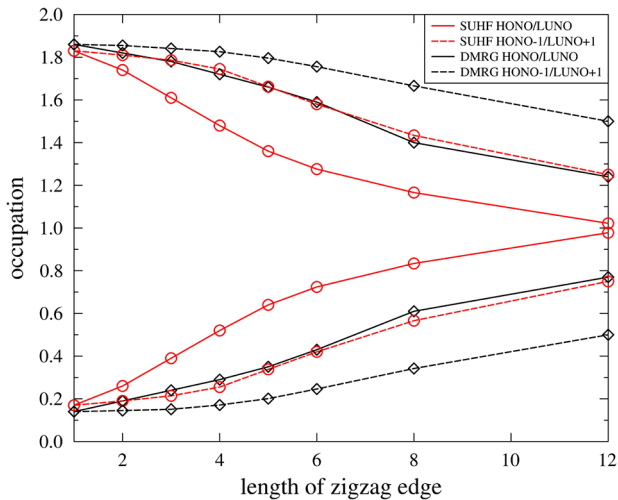


Figure 3. SUHF and DMRG (data taken from ref 4). Natural occupations as a function of the number of acenes with zigzag structures ($W = 1$). CASSCF natural occupations have been used in lieu of DMRG for the case of benzene.

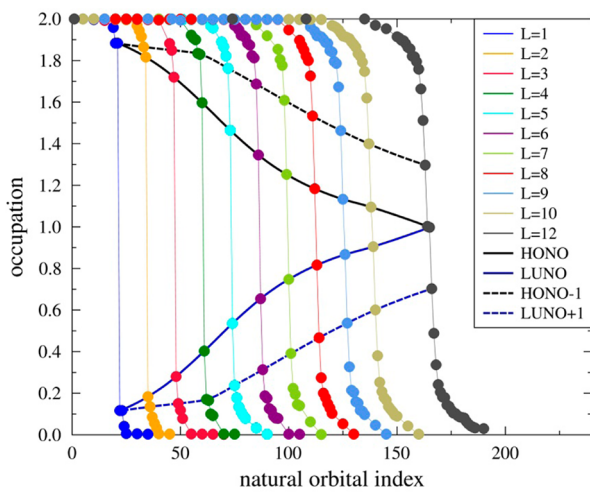


Figure 4. SUHF natural occupations for zigzag edge structures with $W = 1$ and $L = 1-12$ using the 6-31++G(d,p) basis set.

“occupied” to some degree. The natural orbital index used as the abscissa in our Figures is here understood as the index of the eigenvalue (occupation) when orbitals are sorted from highest to lowest occupation.

We start by comparing SUHF with CASSCF and DMRG (available in the literature) results for small polyacene systems to calibrate the performance of our method in studying their polyyradical character. We present in Table 2 a comparison

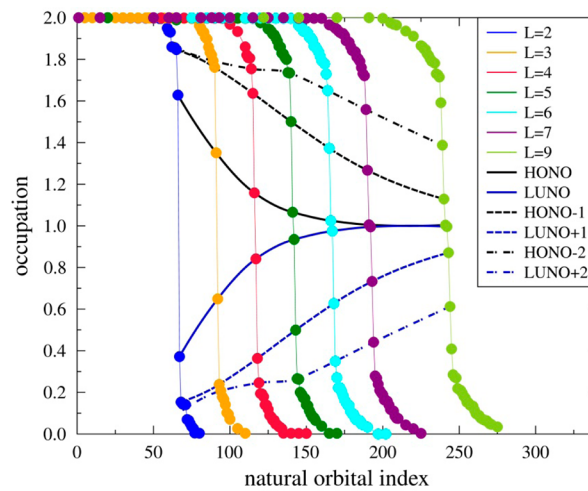


Figure 5. SUHF natural occupations for zigzag edge structures with $W = 2$ and $L = 2-9$ using the 6-31G basis set.

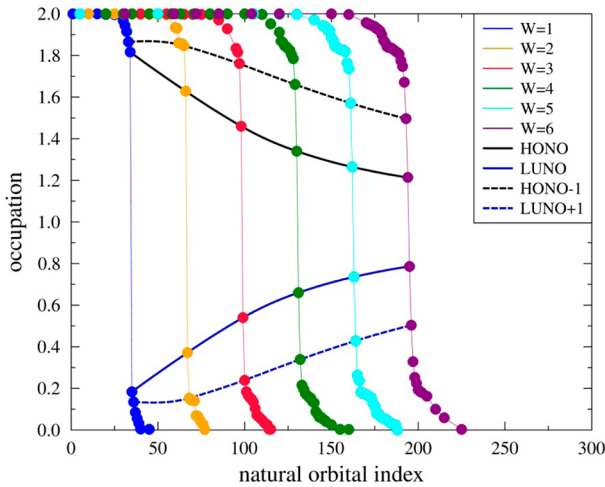


Figure 6. SUHF natural occupations for armchair edge structures with $L = 2$ and $W = 1-6$ using the 6-31G basis set.

between CASSCF, SUHF, and SGHF³⁰ calculations for benzene, naphthalene, and anthracene with the STO-3G basis set. The CASSCF calculations were performed using the full π system as the active space. We have also included results obtained with an active-space-based SUHF;³⁰ we have denoted these with the acronym SUHF*.

We observe that SUHF predicts a lower energy than CASSCF for the benzene molecule, which reflects the ability of SUHF to incorporate correlations from core orbitals. For larger molecules, however, SUHF yields a variational energy

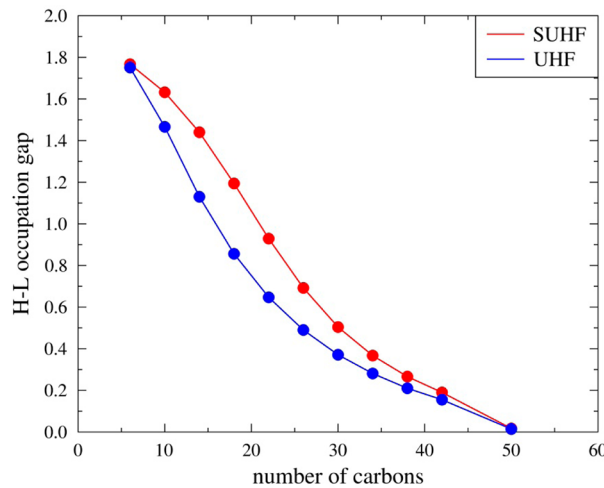


Figure 7. SUHF versus UHF HONO–LUNO occupation gap as a function of the number of carbons for systems with $W = 1$ and $L = 1\text{--}12$ using the 6-31++G(d,p) basis set.

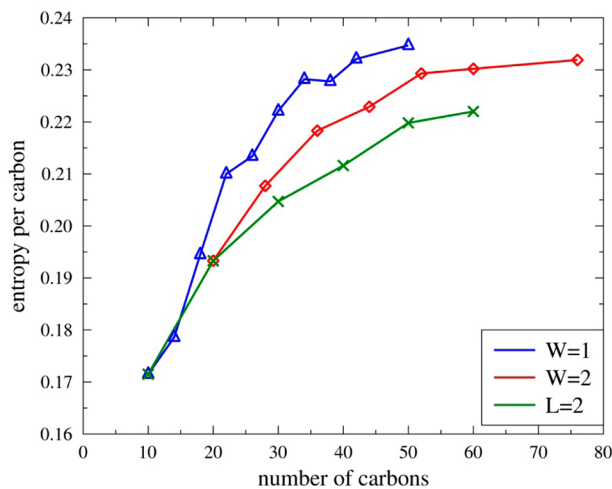


Figure 8. Entropy per carbon versus total number of carbon atoms for three sets of linear acenes with different structural motifs.

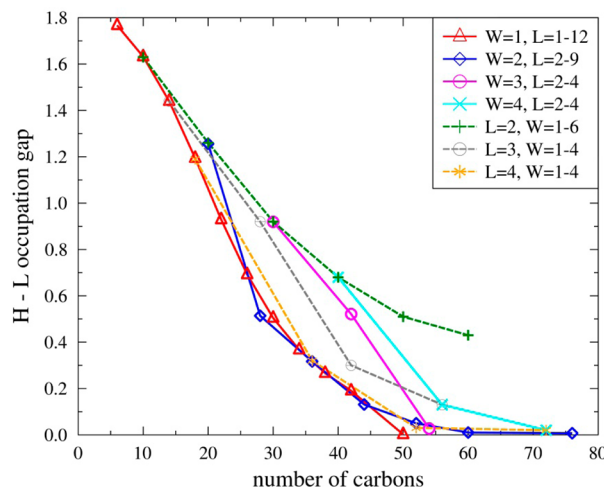


Figure 9. SUHF HONO–LUNO occupation gap versus number of carbon atoms for diverse structures (see the text) using 6-31++G(d,p) ($W = 1$) and 6-31G (other systems).

above that from CASSCF; this is partially a reflection of the size inconsistency of the method. SUHF* calculations were carried out to investigate the ability of SUHF in correlating only active-space electrons. We observe that SUHF* yields higher energies than CASSCF in all cases, as it should; the quality of SUHF* deteriorates for increasingly large systems. In this article, we have used SUHF as a representative projected HF method, allowing the underlying determinant to become generalized HF style,⁴⁶ while doing spin projection in a VAP manner yields the SGHF method. According to the results of Table 2, SGHF yields a lower energy than CASSCF for all systems presented in Table 2. The projected HF method in general can account for a significant fraction of both static and dynamic correlations; the more symmetries that are broken and restored, the higher the quality of the resulting wave function.

In comparing SGHF and CASSCF natural occupations, we observe that they become increasingly dissimilar for larger systems. This may be due, on the one hand, to the restriction to an active space for CASSCF calculations and, on the other hand, to the approximate treatment of electron correlation that SGHF provides. The natural occupations predicted by SUHF* are close to those from SGHF, while a full orbital relaxation in SUHF causes the HONO (LUNO) to become lower (higher). In this sense, SUHF compromises the quality of the 1RDM eigenvalues to account for a larger fraction of the total electron correlation. We finally observe that the tendencies predicted by SUHF are consistent with those of SGHF and CASSCF, even if a quantitative agreement is not reached.

We present in Figure 3 a comparison between the HONO and LUNO obtained with DMRG and SUHF using the STO-3G basis set for systems with $W = 1$. We observe that DMRG predicts, for a given system, higher HONO and LUNO occupations than SUHF does, consistent with the CASSCF results from Table 2. For large systems, DMRG provides a more complete treatment of electron correlation than SUHF, including both static and dynamic, although this is restricted only to the active space used. Nevertheless, results in Figure 3 indicate that SUHF follows a trend similar to DMRG, and thus we deem our results valuable in light of the larger systems and basis sets that can be afforded in our calculations.

Figure 4 shows occupation numbers for oligoacenes ($W = 1$) and $L = 1\text{--}12$, dominated by zigzag edges. Here $L = 1$ corresponds to benzene, $L = 2$ corresponds to naphthalene, and so on. The Figure shows that entanglement increases with the number of acenes (or equivalently, with the number of π electrons). The occupancy of HONO (LUNO) is 1.816 (0.184), 1.597 (0.403), 1.346 (0.654), 1.184 (0.816), 1.095 (0.905), and 1.002 (0.998) for $L = 2, 4, 6, 8, 10$, and 12, respectively. For the longest system ($L = 12$), the HONO and LUNO practically reach single occupancy, in contrast with previous studies. The convergence toward single occupancy may well be an artifact reflecting the limitation of the SUHF method.

Similar trends can be seen in Figure 5 for systems with $W = 2$ and $L = 2\text{--}9$, which are also dominated by zigzag edges. Note that for a given L the number of fused acenes is larger in systems with $W = 2$ than in those with $W = 1$. Single occupancy of the HONO and LUNO orbitals is reached with $L = 7$ (14 acenes). The occupancy of HONO (LUNO) is 1.628 (0.372), 1.159 (0.841), 1.025 (0.975), and 1.005 (0.005) for $L = 2, 4, 6$, and 9, respectively. Note that the series with $W = 2$ adds more carbons as a function of L than the $W = 1$ case, and thus it should not be surprising that the HONO and LUNO converge

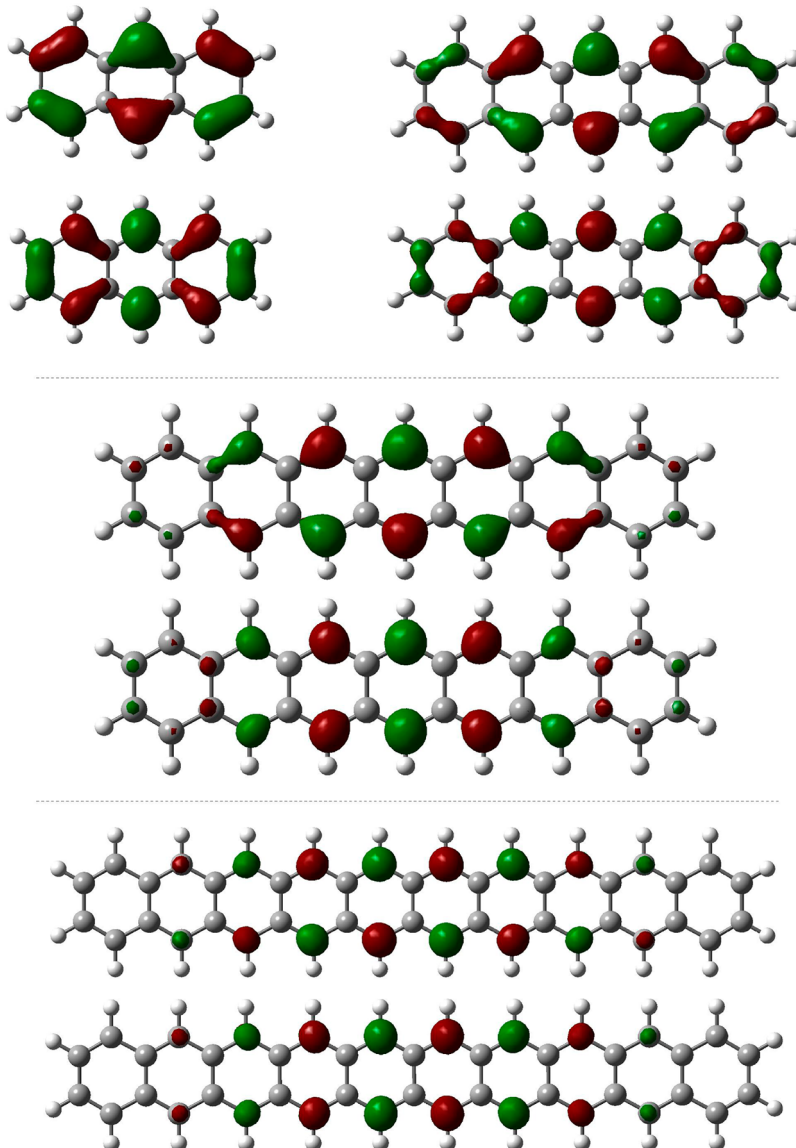


Figure 10. Real-space representation of the HONOs (top) and LUNOs (bottom) for representative members of the $W = 1$ series.

to single occupancy faster. For this series ($W = 2$), Mizukami et al.²⁸ find convergence in the HONO and LUNO occupations with $L = 6$, although their results do not predict that single occupancy is reached. (The LUNO converges to an occupation of ~ 0.75 .)

Results for a series of acenes dominated by armchair edges with $L = 2$ and $W = 1\text{--}6$ are presented in Figure 6. We find that polyradical character as a function of the number of acenes increases more slowly than in the previous cases. Also, HONO and LUNO occupations do not converge to 1 even for large polyacenes. A significant HONO–LUNO occupation gap is observed for these armchair structures. The occupancy of HONO (LUNO) in this series is 1.628 (0.372), 1.340 (0.660), and 1.214 (0.786) for $W = 2, 4$, and 6, respectively.

In light of these results, we conclude that the electronic ground state of PAHs quickly evolves from nonradical singlerefERENCE to polyradical multireference character as a function of the number of acenes (or π -electrons), especially in those dominated by zigzag edges.

We note that the polyradical character displayed in zigzag edges has been described before in terms of spin-polarized

edges by broken-symmetry HF⁴⁷ and DFT calculations.^{18,48} The difference between armchair and zigzag edges in graphene nanoribbons has been discussed⁴⁹ in terms of Clar's empirical theory of aromatic sextets.⁵⁰ In particular, edges admitting Clar's sextets, with armchair edges among them, are predicted to be more stable than others.^{48,51} This agrees with our findings that the HONO and LUNO orbitals tend to localize at zigzag edges (see below) and that it is those orbitals that, for large enough systems, tend toward single occupancy.

We now compare the natural occupations of the UHF and SUHF charge density matrices. (The eigenvalues of the SUHF charge density matrix are equal to those of the full density matrix for spin singlets, for which $\gamma_{\uparrow} = \gamma_{\downarrow}$.) A significant fractional occupancy in UHF natural orbitals has been used previously as a measure of strong correlation.⁵² We present in Figure 7 the HONO–LUNO occupation gap versus the number of carbon atoms for the oligocene series. We observe that for most lengths UHF displays a significantly lower H–L occupation gap compared with SUHF. This occupation gap is a representative way and not necessarily the only way of discerning differences between the UHF and SUHF wave

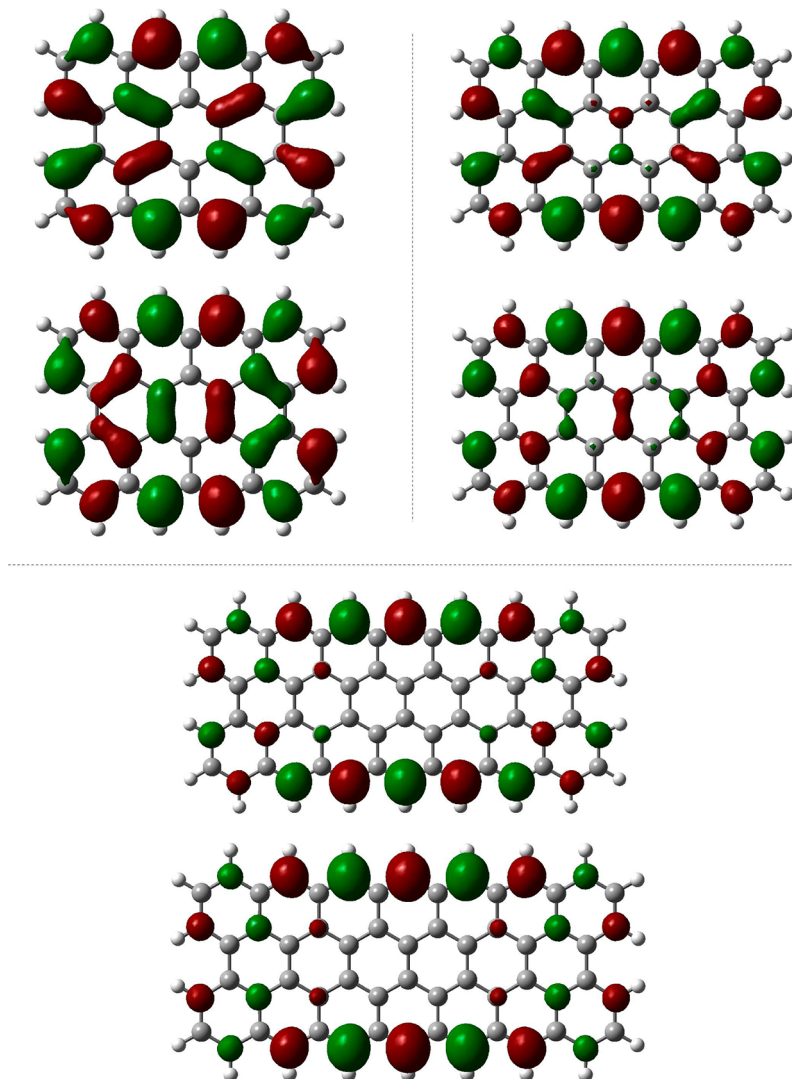


Figure 11. Real-space representation of the HONOs (top) and LUNOs (bottom) for representative members of the $W = 2$ series.

functions. Nevertheless, this result leads us to conclude that even when the correlation energy (with respect to UHF) per acene predicted by SUHF approaches zero for large systems,³⁰ the UHF and SUHF wave functions still have important differences.

Another way of quantifying the multireference character (entanglement) of a system is using the symmetrized von Neumann entropy given by:

$$S = -\frac{1}{2} \sum_i [n_i \ln n_i + (1 - n_i) \ln(1 - n_i)] \quad (9)$$

Here $S = 0$ for a single determinant wave function that has an idempotent one-particle density matrix (i.e., $n_i = 0$ or 1 for all i). The symmetrized entropy given by eq 9 is an extensive quantity; we have therefore chosen to report the symmetrized entropy per carbon atom. Figure 8 presents the symmetrized entropy per carbon versus the total number of carbons for the three structural PAH series previously discussed. The plots indicate that in all cases there is larger entropy per carbon atom as a function of size, although we start observing saturation for the largest systems here analyzed. From this Figure, it is also clear that zigzag edges favor strong correlation.

We have also studied several other systems with even larger L and W . In particular, we have considered the series composed of $W = 1–4$ with growing L and another series of $L = 2–4$ with growing W ; this is equivalent to extending zigzag edges (by setting W) or extending armchair edges (by setting L), respectively. The largest representatives of these families were presented above in Table 1. Figure 9 shows the evolution of the HONO–LUNO occupation gap with the number of carbon atoms for all series studied in this paper. The plot indicates that the fastest development of strong correlation is seen in the $W = 1$ series. As the width increases, the polyyradical character observed is smaller for a given number of carbons. The opposite trend happens for the series with varying length ($L = 2, 3, 4$). In this case, the polyyradical character is bigger with increasing L for a given number of carbon atoms. We conclude that strong correlation is favored by linearly fused acenes in structures with zigzag edges. Increasing the width of the strips does not enhance entanglement.

Finally, we explore the real-space representation of the HONO and LUNO of a select group of PAHs with the aim of rationalizing differences in emergent polyyradical character between systems with zigzag and armchair edges. For the series with $W = 1$, Figure 10 shows the progressive localization

of both HONOs and LUNOs on the molecular center edges as the length increases. Edge localization is also observed in Figure 11 for the $W = 2$ series, with a clearly decreasing contribution from the PAH center. In general, we observe preference of HONO and LUNO localization on zigzag over armchair edges. This effect is clear and pronounced in the $W = 4$, $L = 4$ structure already presented in Figure 1. In most cases, the HONO displays more nodal planes along the zigzag edges than the LUNO, consistent with the fact that it has a higher occupation. It is interesting to note that the plots presented in Figures 10 and 11 are reminiscent of those obtained with symmetry-broken screened hybrid density functional theory for the spin density;⁵³ in the present work, however, the SUHF spin density is everywhere zero, as it should be for any true spin singlet.

CONCLUSIONS

We have studied orbital entanglement and polyyradical character on a series of polyaromatic hydrocarbons using our recently developed SUHF method. Accurate modeling of these molecules must rely on methods capable of handling strong correlations with large basis sets. Studying large structures requires affordable computations. Because SUHF delivers the two treats of computational speed and multireference character, it seems poised to become an interesting option for tackling other similar problems in chemistry. In SUHF, strong correlations arising from spin fluctuations are naturally accounted for by means of the projection formalism. Nevertheless, the connection with a single-particle picture is not lost, as one can still easily grasp the relevant physics in the optimized broken-symmetry determinant.

Our calculations suggest that entanglement and polyyradical character are both strongly dependent on molecular size and structural motif. In all cases studied, we have observed an increase in entanglement as a function of the number of acenes. More specifically, systems with zigzag edges and $W = 1, 2$ show the fastest development of polyyradical behavior, achieving single occupancy when the system reaches about 50 carbon atoms independently of the number of acenes. Conversely, the HONO–LUNO occupation gap of armchair edge structures converges more slowly.

AUTHOR INFORMATION

Corresponding Author

*E-mail: jr34@rice.edu. Phone: +(001) 713-348-2657.

Notes

The authors declare no competing financial interest.

ACKNOWLEDGMENTS

This work was supported by the Department of Energy, Office of Basic Energy Sciences, grant no. DE-FG02-09ER16053. G.E.S. is a Welch Foundation Chair (C-0036).

REFERENCES

- (1) Clar, E. *Polyyclic Hydrocarbons*; Academic Press: London, 1964; Vol. 1, p 2.
- (2) Bendikov, M.; Duong, H. M.; Starkey, K.; Houk, K. N.; Carter, E. A.; Wudl, F. Oligoacenes: Theoretical Prediction of Open-Shell Singlet Diradical Ground States. *J. Am. Chem. Soc.* **2004**, *126*, 7416–7417.
- (3) Hajgató, B.; Szieberth, D.; Geerlings, P.; De Proft, F.; Deleuze, M. S. A Benchmark Theoretical Study of the Electronic Ground State and of the Singlet-Triplet Split of Benzene and Linear Acenes. *J. Chem. Phys.* **2009**, *131*, 224321.
- (4) Hachmann, J.; Dorando, J. J.; Avilés, M.; Chan, G. K.-L. The Radical Character of the Acenes: A Density Matrix Renormalization Group Study. *J. Chem. Phys.* **2007**, *127*, 134309.
- (5) Hajgató, B.; Huzak, M.; Deleuze, M. S. Focal Point Analysis of the Singlet-Triplet Energy Gap of Octacene and Larger Acenes. *J. Phys. Chem. A* **2011**, *115*, 9282–9293.
- (6) Bettinger, B. Electronic Structure of Higher Acenes and Polyacene: The Perspective Developed by Theoretical Analyses. *Pure Appl. Chem.* **2010**, *82*, 905–915.
- (7) Yamashita, Y. Organic Semiconductors for Organic Field-Effect Transistors. *Sci. Technol. Adv. Mater.* **2009**, *10*, 024313–024321.
- (8) Boström, C.-E.; Gerde, P.; Hanberg, A.; Jernström, B.; Johansson, C.; Kyrklund, T.; Rannug, A.; Törnqvist, M.; Victorin, K.; Westerholm, R. Cancer Risk Assessment, Indicators, and Guidelines for Polycyclic Aromatic Hydrocarbons in the Ambient Air. *Environ. Health Perspect.* **2002**, *110*, 451–488.
- (9) Klauk, H.; Halik, M.; Zschieschang, U.; Eder, F.; Schmid, G.; Dehm, C. Pentacene Organic Transistors and Ring Oscillators on Glass and on Flexible Polymeric Substrates. *Appl. Phys. Lett.* **2003**, *82*, 4175–4177.
- (10) Payne, M. M.; Parkin, S. R.; Anthony, J. E. Organic Field-Effect Transistors from Solution-Deposited Functionalized Acenes with Mobilities as High as $1\text{cm}^2/\text{V s}$. *J. Am. Chem. Soc.* **2005**, *127*, 8028–8029.
- (11) Mondal, R.; Shah, B. K.; Neckers, D. C. Photo-Generation of Heptacene in a Polymer Matrix. *J. Am. Chem. Soc.* **2006**, *128*, 9612–9613.
- (12) Zade, S. S.; Bendikov, M. Heptacene and Beyond: The Longest Characterized Acenes. *Angew. Chem., Int. Ed.* **2010**, *49*, 4012–4015.
- (13) Pelzer, K.; Greenman, L.; Gidofalvi, G.; Mazzotti, D. The Multiradical Character of One- and Two-Dimensional Graphene Nanoribbons. *J. Phys. Chem. A* **2011**, *115*, 5632–5640.
- (14) Hummer, K.; Ambrosch-Draxl, C. Oligoacene Exciton Binding Energies: Their Dependence on Molecular Size. *Phys. Rev. B* **2005**, *71*, 81202.
- (15) Anthony, J. E. Functionalized Acenes and Heteroacenes for Organic Electronics. *Chem. Rev.* **2006**, *106*, 5028–5048.
- (16) Jiang, D.; Sumpter, B.; Dai, S. Unique Chemical Reactivity of a Graphene Nanoribbon's Zigzag Edge. *J. Chem. Phys.* **2007**, *126*, 134701.
- (17) Hod, O.; Barone, V.; Peralta, J. E.; Scuseria, G. E. Enhanced Half-Metallicity in Edge-Oxidized Zigzag Graphene Nanoribbons. *Nano Lett.* **2007**, *7*, 2295–2299.
- (18) Hod, O.; Peralta, J. E.; Scuseria, G. E. Edge Effects in Finite Elongated Graphene Nanoribbons. *Phys. Rev. B* **2007**, *76*, 233401.
- (19) Barone, V.; Hod, O.; Peralta, J. E.; Scuseria, G. E. Accurate Prediction of the Electronic Properties of Low-Dimensional Graphene Derivatives Using a Screened Hybrid Density Functional. *Acc. Chem. Res.* **2011**, *44*, 269–279.
- (20) Bally, T.; Borden, W. T. A Review of Calculations on Open Shell Species (Doublets and Triplets). *Rev. Comput. Chem.* **1999**, *13*, 1–97.
- (21) Stanton, J. F.; Gauss, J. A Discussion of some Problems Associated with the Quantum Mechanical Treatment of Open-Shell Molecules. *Adv. Chem. Phys.* **2003**, *125*, 101–146.
- (22) Kadantsev, E. S.; Stott, M. J.; Rubio, A. Electronic Structure and Excitations in Oligoacenes from Ab Initio Calculations. *J. Chem. Phys.* **2006**, *124*, 134901.
- (23) Aiga, F. Theoretical Study on Oligoacenes and Polycyclic Aromatic Hydrocarbons using the Restricted Active Space Self-Consistent Field Method. *J. Phys. Chem. A* **2012**, *116*, 663–669.
- (24) Mazzotti, D. A. *Reduced-Density-Matrix Mechanics with Application to Many-Electron Atoms and Molecules*; Wiley: New York, 2007.
- (25) Greenman, L.; Mazzotti, D. A. Highly Multireferenced Arynes Studied with Large Active Spaces Using Two-Electron Reduced Density Matrices. *J. Chem. Phys.* **2009**, *130*, 184101.

- (26) Sinitskiy, A.; Greenman, L.; Mazziotti, D. A. Strong Correlation in Hydrogen Chains and Lattices Using the Variationa Two-Electron Reduced Density Matrix Method. *J. Chem. Phys.* **2010**, *133*, 014104.
- (27) Gidofalvi, G.; Mazziotti, D. A. Active-Space Two-Electron Reduced-Density-Matrix Method: Complete Active-Space Calculations without Diagonalization of the N-Electron Hamiltonian. *J. Chem. Phys.* **2008**, *129*, 134108.
- (28) Mizukami, W.; Kurashige, Y.; Yanai, T. More π Electrons Make a Difference: Emergence of Many Radicals on Graphene Nanoribbons Studied by Ab Initio DMRG Theory. *J. Chem. Theory Comput.* **2013**, *9*, 401–407.
- (29) Plasser, F.; Pašalić, H.; Gerzabek, M. H.; Libisch, F.; Reiter, R.; Burgdörfer, J.; Müller, T.; Shepard, R.; Lischka, H. The Multiradical Character of One- and Two-Dimensional Graphene Nanoribbons. *Angew. Chem., Int. Ed.* **2013**, *S2*, 36–39.
- (30) Jiménez-Hoyos, C. A.; Henderson, T. M.; Tsuchimochi, T.; Scuseria, G. E. Projected Hartree-Fock Theory. *J. Chem. Phys.* **2012**, *136*, 164109.
- (31) Strout, D. L.; Scuseria, G. E. A Quantitative Study of the Scaling Properties of the Hartree-Fock Method. *J. Chem. Phys.* **1995**, *102*, 8448–8452.
- (32) Samanta, K.; Jiménez-Hoyos, C. A.; Scuseria, G. E. Exploring Copper Oxide Cores using Projected Hartree-Fock Theory. *J. Chem. Theory Comput.* **2012**, *8*, 4944–4949.
- (33) Rodríguez-Guzmán, R.; Schmid, K. W.; Jiménez-Hoyos, C. A.; Scuseria, G. E. Symmetry-Projected Variational Approach for Ground and Excited States of the Two-Dimensional Hubbard Model. *Phys. Rev. B* **2012**, *85*, 245130.
- (34) Peschel, I. Lecture notes for the Brazilian School on Statistical Mechanics. *Braz. J. Phys.* **2012**, *42*, 267–291.
- (35) Löwdin, P.-O. Quantum Theory of Many-Particle Systems. III. Extension of the Hartree-Fock Scheme to Include Degenerate Systems and Correlation Effects. *Phys. Rev.* **1955**, *97*, 1509–1520.
- (36) Goddard, W. A. Improved Quantum Theory of Many-Electron Systems. *J. Chem. Phys.* **1968**, *48*, 450–461.
- (37) Mayer, I. The Spin Projected Hartree-Fock Method. *Adv. Quantum Chem.* **1980**, *12*, 189–262.
- (38) Schlegel, H. B. Potential Energy Curves using Unrestricted Møller-Plesset Perturbation Theory with Spin Annihilation. *J. Chem. Phys.* **1986**, *84*, 4530–4534.
- (39) San-Fabián, E.; Moscardó, F. On the Actual Nature of the Anti-Ferromagnetism shown by Unrestriced Calculations on Conjugated Hydrocarbon Rings. *Eur. Phys. J.* **2011**, *64*, 239–248.
- (40) Scuseria, G. E.; Jiménez-Hoyos, C. A.; Henderson, T. M.; Samanta, K. Projected Quasiparticle Theory for Molecular Electronic Structure. *J. Chem. Phys.* **2011**, *135*, 124108.
- (41) Rodríguez-Guzmán, R.; Egido, J. L.; Robledo, L. M. Correlations Beyond the Mean Field in Magnesium Isotopes: Angular Momentum Projection and Configuration Mixing. *Nucl. Phys. A* **2002**, *709*, 201–235.
- (42) Harriman, J. E. Natural Expansion of the First-Order Density Matrix for a Spin-Projected Single Determinant. *J. Chem. Phys.* **1964**, *40*, 2827.
- (43) Frisch, M. J.; Trucks, G. W.; Schlegel, H. B.; Scuseria, G. E.; Robb, M. A.; Cheeseman, J. R.; Scalmani, G.; Barone, V.; Mennucci, B.; Petersson, G. A., et al. *Gaussian Development Version*, revision H.1; Gaussian, Inc.: Wallingford, CT, 2009.
- (44) Pulay, P. Convergence Acceleration in Iterative Sequences: The Case of SCF Iteration. *Chem. Phys. Lett.* **1980**, *73*, 393–398.
- (45) Scuseria, G. E.; Lee, T. J.; Schaefer, H. F. Accelerating the Convergence of the Coupled Cluster Approach: The Use of the DIIS Method. *Chem. Phys. Lett.* **1986**, *130*, 236.
- (46) Jiménez-Hoyos, C. A.; Henderson, T. M.; Scuseria, G. E. Generalized Hartree-Fock Description of Molecular Dissociation. *J. Chem. Theory Comput.* **2011**, *7*, 2667–2674.
- (47) Yamashiro, A.; Shimoni, Y.; Harigaya, K.; Wakabayashi, K. Spin- and Charge-polarized states in Nanographene Ribbons with Zigzag Edges. *Phys. Rev. B* **2003**, *68*, 193410.
- (48) Pisani, L.; Chan, J. A.; Montanari, B.; Harrison, N. M. Electronic and Magnetic Properties of Graphitic Ribbons. *Phys. Rev. B* **2007**, *75*, 064418.
- (49) Wassmann, T.; Seitsonen, A. P.; Saitta, A. M.; Lazzeri, M.; Mauri, F. Clar's Theory, pi-Electron Distribution, and Geometry of Graphene Nanoribbons. *J. Am. Chem. Soc.* **2010**, *132*, 3440–3451.
- (50) Gutman, I.; Tomović, Ž.; Müllen, K.; Rabe, J. P. On the Distribution of π -Electrons in Large Polycyclic Aromatic Hydrocarbons. *Chem. Phys. Lett.* **2004**, *397*, 412–416.
- (51) Balavan, A. T.; Klein, D. J. Claromatic Carbon Nano-Structures. *J. Phys. Chem. C* **2009**, *113*, 19123–19133.
- (52) Pulay, P.; Hamilton, T. P. UHF Natural Orbitals for Defining and Starting MC-SCF Calculations. *J. Chem. Phys.* **1988**, *88*, 4926–4933.
- (53) Hod, O.; Barone, V.; Scuseria, G. E. Half-Metallic Graphene Nanodots: A Comprehensive First-Principles Theoretical Study. *Phys. Rev. B* **2008**, *77*, 035411.